Journal of Asian Ceramic Societies 3 (2015) 417–425

HOSTED BY

Contents lists available at ScienceDirect

Journal of Asian Ceramic Societies

journal homepage: www.elsevier.com/locate/jascer

Electrospun of polymer/bioceramic nanocomposite as a new soft tissue for biomedical applications

Hamid Amiri Heydary[a], Ebrahim Karamian[b], Elahe Poorazizi[c], Jalil Heydaripour[d], Amirsalar Khandan[e,*]

[a] Department of Tissue Engineering, Najafabad Branch, Islamic Azad University, Najafabad, Isfahan, Iran
[b] Advanced Materials Research Center, Faculty of Materials Engineering, Najafabad Branch, Islamic Azad University, Najafabad, Isfahan, Iran
[c] Department of Biochemistry, Faculty of Medicine, Najafabad Branch, Islamic Azad University, Najafabad, Isfahan, Iran
[d] Chemistry Department, Eastern Mediterranean University, North Cyprus, Gazimağusa, TRNC, Mersin 10, Turkey
[e] Mechanical Engineering Department, Eastern Mediterranean University, North Cyprus, Gazimağusa, TRNC, Mersin 10, Turkey

ARTICLE INFO

Article history:
Received 7 June 2015
Received in revised form
20 September 2015
Accepted 24 September 2015
Available online 23 October 2015

Keywords:
Gum Tragacanth
PVA
Electrospinning
Tissue engineering
Bioactivity

ABSTRACT

Iranian Gum Tragacanth (IGT) is among the most natural polymers which has interesting properties such as nontoxic nature, biodegradability and high resistance to bacterial attacks making it applicable for tissue scaffolds, protective clothing, and wound healing. In the current work, polyvinyl alcohol (PVA)/IGT nanocomposite fibre is prepared by using the electrospinning (ELS) technique in an aqueous solution with different volume ratios of 60/40, 70/30, 80/20, and 90/10. To enhance the chemical and mechanical stability of the produced samples, different amounts of nanoclay powder (1% and 3%) are added also to the solution. The blended nanofibres are characterized by scanning electron microscopy (SEM), Fourier-transform infrared (FTIR), and bioactivity evaluation in phosphate buffered saline (PBS) and simulated body fluid (SBF) solutions. The FTIR analysis indicated that PVA and IGT may have H^+ bonding interactions. The results revealed that with a higher amount of IGT, a superior degradation as well as a higher chemical and biological stability could be obtained in the nanobiocomposite blend fibres. Furthermore, the blend nanofibre samples of 80/20 and 3% nanoclay powder exhibit a significant improvement during evaluation of its properties.

1. Introduction

In the last two decades there has been a growing interest in biocompatible and biodegradable natural polymers that are being used as scaffolds and in wound healing for tissue engineering [1]. To design soft and hard scaffolds, the main requirements are high porosity, higher wettability, large surface area, and a microenvironment that allows the cells to adhere, proliferate, differentiate, and retain its phenotype [2]. It is well established that pores fibres, which are interconnected, play an important role in cellular growth [3]; however, with increasing porosity, an inevitable loss occurs in the biological properties [4]. A large number of different polymers including hydrogels polyvinyl alcohol (PVA) [5], polyacrylamide (PAC) [6], and polyacrylic acid (PAA) [7] have been explored for different biomaterials applications [8].

Among these, PVA has been used for various pharmaceutical applications [9]. Some of the advantages of PVA are its nontoxicity, excellent physical properties, high hydrophilicity, biocompatibility, good chemical resistance, and bioadhesive nature making it a suitable candidate for regenerative medicine especially wound healing applications [10]. It also showed a high degree of swelling in water, and an elastic nature which can closely simulate natural tissue so that it can be readily accepted by the body [11].

Another known polymer, local Iranian Gum Tragacanth (IGT), is a dried exudation obtained from the stems and branches of Asiatic species of Astragalus [12]. It has been used as an emulsifier and pharmaceutical for wound healing applications. The IGT is one of the most acid-resistance gums and most efficient natural emulsifier for acidic oil-in-water emulsions [13]. The IGT and PVA represent renewable sources and they have no adverse impact on skin and eye irritation [14].

Due to their unique characteristics and potential commercial applications, polymers have been composited with new generation

* Corresponding author. Tel.: +90 5338529577.
E-mail address: Amirsalar.khandan@cc.emu.edu.tr (A. Khandan).
Peer review under responsibility of The Ceramic Society of Japan and the Korean Ceramic Society.

http://dx.doi.org/10.1016/j.jascer.2015.09.003

of bioceramics and have brought improved mechanical properties. The nanoclay (NC), as a famous bioceramic, has recently been taken into consideration due to its good mechanical properties [15,26]. Adding NC to biopolymer-based nanocomposites improves their mechanical, biological, chemical, thermal [16,17], and corrosion protection properties [18].

Nanofibres can be obtained by a number of techniques comprised of air-blast atomization of mesophase pitch [19–22], assembling from individual CNT molecules [20], pulling of nonpolymer [21] and depositing materials on linear templates [22]. Electrospinning (ELS) technique as a popular technique to prepare soft tissues is not only applicable due to its versatility in spinning a wide variety of polymeric fibres but also due to its consistency in producing fibres in the submicron range wound healing [23]. Despite the poor mechanical properties of natural polymer nanocomposites, its unique biological properties lead us to focus on improving its properties rather than completely replacing it with other biopolymers. Accordingly, in this work we have prepared a new IGT-PVA nanocomposite as a highly bioactive material for wound healing applications and have evaluated its *in vitro*, chemical as well as mechanical properties.

2. Material and methods

2.1. Materials

PVA and nanoclay powder were purchased from Merck (Co., Germany) and milled by mechanical milling (MM) technique. First of all, in order to homogenize the nanoclay (NC) powder, it was ball milled for 2 h with a planetary mill comprised of zirconia vial and balls in which a ball to powder weight ratio (BPR) of 15 and rotational speed of 600 rpm were used.

X-ray fluorescence (XRF) analysis of the nanoclay is shown in Table 1. This table shows that silicon (Si) has the highest amount of the element ratio in the composition.

In this study, the IGT with high quality ribbon type was collected from plants growing in the mountainous areas (Isfahan Province, Iran). Pure powdered IGT with a mesh size between 80 and 400 was used in this study. All other chemical reagents for preparation of bioactivity solution were obtained from Merck (Germany)-grade including NaCl (99.5%), $NaHCO_3$ (99.5%), KCl (99.0%), $Na_2HPO_4{\cdot}3H_2O$ (99.5%), $MgCl_2{\cdot}6H_2O$ (98.0%), Na_2SO_4, $(CH_2OH)_3CNH_2$ (99.2%), $CaCl_2{\cdot}2H_2O$ (99.0%) and HCl (37 vol%).

2.2. Purification of IGT

The primary IGT was washed by deionized water and dried in sunlight; after that it was milled and sieved. The density value of IGT was 1/42 g/cm^3. The 4 g of IGT was dissolved in deionized water and homogenized on the magnetic stirring overnight and then allowed to stay for 12 h at room temperature. The mucilage was filtrated and separated through a glass funnel. The obtained clear solution was dried through freeze-drying, and weighted and stored. A schematic of the whole process to prepare IGT is shown in Fig. 1.

2.3. Composite preparation

The polymer solution was prepared by dissolving different ratios 90:10, 80:20, 70:30, 60:40 of PVA/IGT in 100 ml of deionized water. We selected an 80:20 ratio of PVA/IGT, as it obtained a maximum solubility in comparison with other solvents used for electrospinning. The NC in different concentrations, 0.0%, 1%, and 3% (w/w), was used. The effect of NC on the nanobiopolymers was investigated by FTIR analysis. The homogenized NC was then slowly added to the PVA/IGT solution with stirring process at room temperature. The solution was allowed to stir for 30 min in a sealed container and the obtained mixture was further sonicated for 5 min.

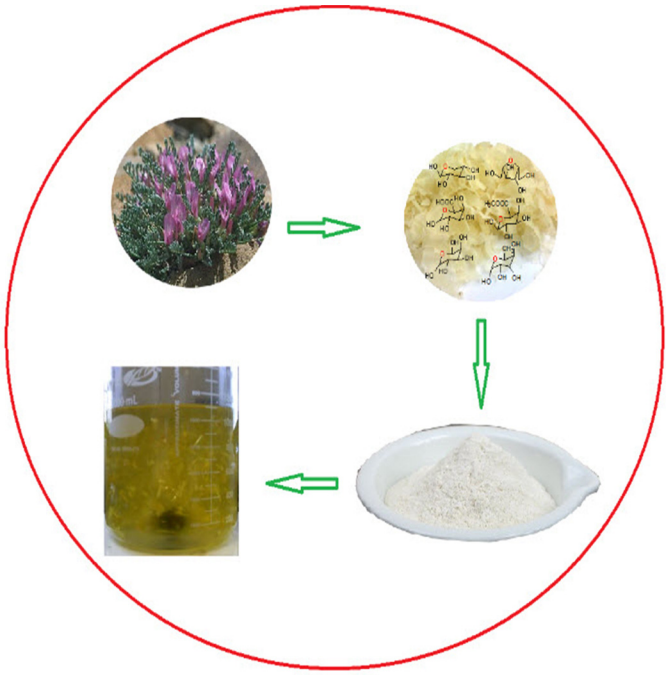

Fig. 1. The schematic of IGT preparation from Iranian plant to natural polymer (plants, dried IGT, IGT powder, IGT dissolved).

2.4. Electrospinning (ELS) method

ELS technique is one of the most important approaches for developing continuous nanoscale fibres with diameters ranging from 10 to 50 nm. After that, the solution was stirred for 8 h, the NC was added to it and again the stirring process went on up to 10 h. The obtained solution was then stored at 4 °C for 6 h to reach the required homogeneity. The biocomposite solution was fed into a 20 ml plastic syringe fitted with a needle. The ELS of PVA/IGT with different percentages of NC-enriched was carried out by a syringe pump using a feeding rate of 0.5–1.5 ml/h (flow rate) and a voltage of 10–20 kV. The collector plate was made of aluminium (Al) foil; the dimension of frame was 10 mm × 50 mm which was positioned at a constant distance of 10 cm from the needle. The fabricated soft scaffolds were dried overnight in vacuum to remove their residual solvent. The ELS procedure (compositing, syringe pump, and electrospun on aluminium) is shown in Fig. 2.

2.5. Bioactivity test

The bioactivity test can be referred to a method that is used for monitoring the bioactivity of nanobiocomposite, during which the samples are soaked in the simulated body fluids (SBF). The reliability of the SBF test depends on the type of bioceramic and

Table 1
XRF of chemical composition nanoclay powder synthesized by MA process.

Composition (wt.%)	CaO	SiO_2	Al_2O_3	Fe_2O_3	MgO	SO_3	Na_2O	K_2O	TiO_2	P_2O_5	Total	Ignition loss
Kaolin	0.17	61.25	20.95	6.40	0.38	0.17	1.61	0.72	0.72	0.12	92.38	13.65

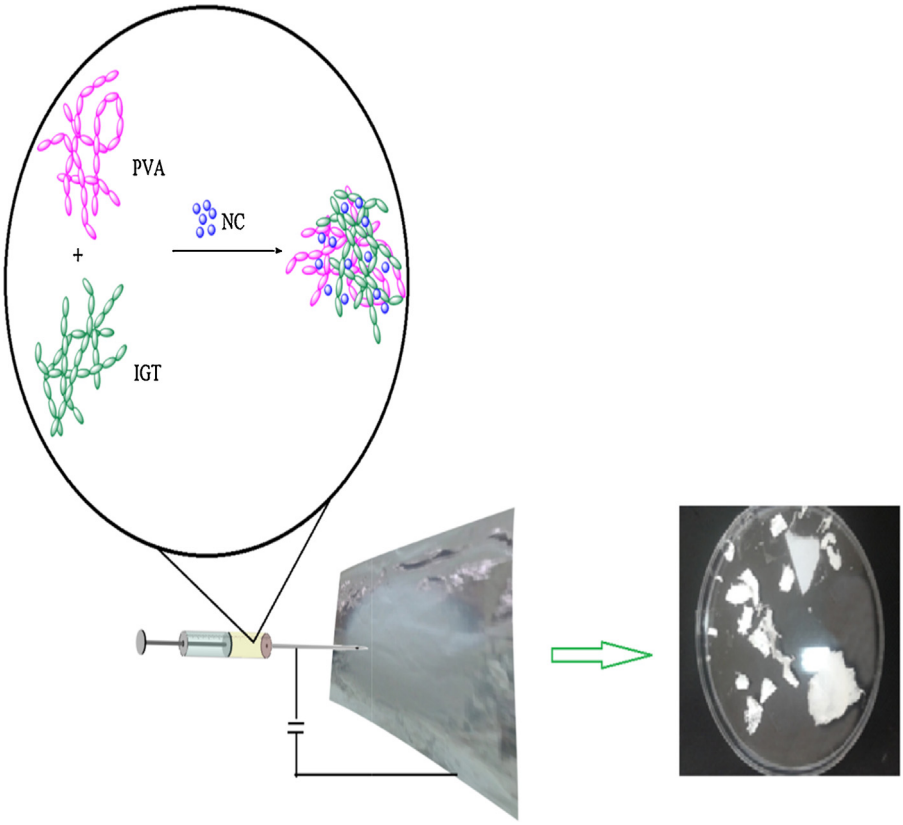

Fig. 2. The electrospinning method used to produce nanobiocomposite (IGT/PVA–NC).

biopolymer used. Natural polymer and silicate-based ceramics reveal excellent ability to form apatite layers on the surface of the hard and soft tissues. Table 2 represents the ion concentration in the SBF solution which has been developed in accordance with Kokubo's method and also its comparison with human blood plasma. According to the Kokubo's method, the essential requirement for a material to bond to the living bone is the formation of bone-like apatite on its surface when it is implanted in the living body. Nanobiocomposite samples were soaked in the SBF solution for the given times of 1, 7, 14, 21 and 28 days at 37 °C with pH = 7.4, without refreshing the soaking medium [24–26]. After these periods, the samples were taken out and dried at 60 °C for 1 h and then re-weighed.

2.6. Degree of swelling and weight loss

The degree of the weight loss of the nanofibre samples was calculated by the use of Eq. (1). The test is carried out in the release medium (phosphate buffered saline, PBS, pH 7.4) at 37 °C for 1, 4, and 28 days. The PBS solution was prepared by dissolving the NaCl (8 g), KCl (0.2 g), Na_2HPO_4 (1.44 g), and KH_2PO_4 (0.24 g) in 800 ml deionized water. The pH of PBS prepared at room temperature has to be adjusted at 7.4 with HCl, 1 M and final volume of 1 l with additional distilled water. Finally, IGT/PVA solution is sterilized by autoclaving and stored in regenerator at 5 °C. *In vitro* degradation of porous scaffolds was carried out in PBS solution according to ASTM F 163 T 044 standard method (60). The porous scaffolds were located in a 20 ml falcon bottle containing 20 ml PBS solution. The produced samples were then placed in an electrical water bath at 37 ± 1 °C for 5 weeks. Every four days, the pH of the PBS solution was measured by pH metre and then replaced with fresh PBS. These experiments were carried out in one month. Biweekly, three samples of each scaffold type were taken out from the falcon bottles for characterization. Lost weight was calculated by this formula

$$\text{Weight loss percentage} = \frac{W_0 - W_t}{W_0} \quad (1)$$

W_0 = initial dry weight sample and W_t = dry weight sample after specific time.

Table 2
Comparison of nominal ion concentrations of SBF, physiological saline, and human blood plasma.

Ion	SBF [mmol]	Human plasma [mmol]
Na^+	142.0	142.0
K^+	5.0	5.0
Mg^{2+}	1.5	1.5
Ca^{2+}	2.5	2.5
Cl^-	147.8	103.0
HCO_3^-	4.2	27.0
HPO_4^{2-}	1.0	1.0
SO_4^{2-}	0.5	0.5
pH	7.4	7.2–7.4

2.7. Mechanical properties

The mechanical properties of fibres including tensile strength and elongation at fracture point are measured by tensile machine (zwick 1446-60, Germany).

2.8. Characterization of the composite

2.8.1. X-ray diffraction

X-ray diffraction (XRD) patterns were revealed with a Pan Analytical Model X'Pert Pro which had CuKα, (λ = 0.1542 nm) Bruker AXS Germany. The diffractograms were recorded in the 2θ range of 20–50° with step size of 0.02 Å and a step time of 0.605.

Table 3
BET and surface area parameter.

Sample	Weight (g)	S(BET) (m^2/g)	S(total) (m^2)
GP_0	0.027	5.150	0.060
GP_3	0.116	6.079	0.164

2.8.2. Fourier transform infrared spectroscopy

In order to investigate the possible changes in chemical composition nanofibre, the FTIR (Perkin-Elmer, UK wave number range of 650–3500 with 4 cm^{-1} resolution) was used.

2.8.3. BET analysis

The surface area measurements were interpreted by the model presented by Brunauer, Emmett and Teller (BET). These measurements are based on the physical adsorption of gas on the sample surface. The amount of gas can be defined by the Langmuir isotherm. The BET is calculated by Eq. (2).

The evaluation of the particle size distribution was performed by PSA analysis (model Malvern instruments, Isfahan Medical university) to discover the nanocrystalline shape and size. The PSA technique that was used to recognize geometric shape of NC nanoparticles is shown in Table 3. The conditions during PSA analysis were a temperature of 19.9 °C, duration time of 70 s and ethanol as a dispersant [viscosity (cp = 1.2000)]. The average particle size of the prepared powder assuming the synthesized nanoparticle was spheroid and is given by Eq. (2),

$$D = \frac{6000}{S(\mathrm{BET}) \times \rho} \quad (2)$$

The composites porosity was measured by Archimedes method. The porosity was calculated according to the following equation:

$$\text{Porosity} = \frac{(W_2 - W_1)}{(W_2 - W_3)} \times 100\% \quad (3)$$

in which W_1 is the weight of composite in air, W_2 is the weight of sample with water, and W_3 is the weight of samples suspended in water.

2.8.4. SEM/EDS analysis

The morphology of the fibrous membrane was observed with a scanning electron microscope SEM (Philips XL30, Eindhoven, and Netherlands). All of the samples were coated with gold (Au) using spraying, high vacuum and 40 kV accelerating voltage. Ion contents were measured from five spots, and the average was measured. The energy-dispersive X-ray spectroscopy (EDS) microanalysis (FEI Quanta 200 ESEM equipped with an EDX EDS device) was also used to verify the accuracy of the experimental results; the nanofibre diameter ($SD_{\text{nanofibre diameter}}$ = 5 nm) measurements were performed two times and the typical standard deviation was 3–5 nm.

2.8.5. Inductive coupled plasma atomic emission spectroscopy

The concentrations of Ca, Si, ... ions in SBF after soaking were determined using inductive coupled plasma atomic emission spectroscopy (ICP-AES; Zaies 110394c).

2.8.6. X-ray fluorescence spectrometry

The elemental analysis of NC powder (raw material) is performed by X-ray fluorescence spectrometry (XRF, Bruker-S4 Pioneer, and Germany).

2.9. Statistical analysis

The statistic SPSS data were analysed with SPSS 20.0 software (SPSS Inc., IL, USA). All values were expressed as mean plus or minus standard deviation. Analysis of variance (ANOVA) was also used to analyse the experimental data. Statistical significance was set to $p < 0.05$. The fibre diameter measurement values were obtained by digitizer software and analysed by using SPSS software.

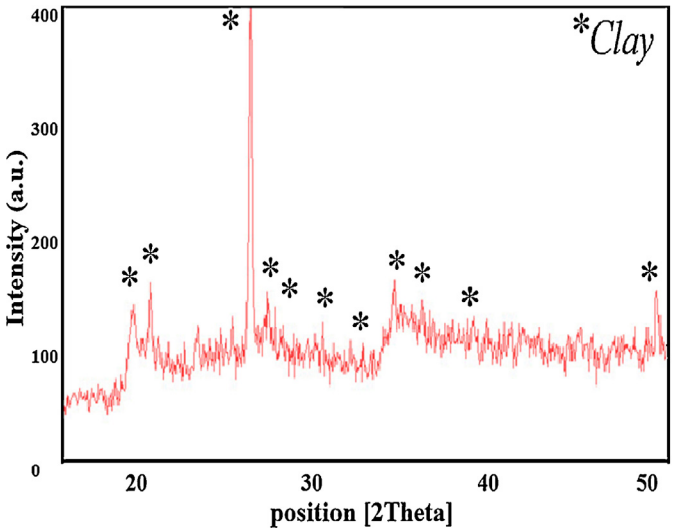

Fig. 3. XRD pattern of NC powder milled for 2 h in a high-energy planetary ball mill.

3. Results and discussion

3.1. X-ray diffraction (XRD)

Fig. 3 indicates the XRD patterns of the NC powder milled for 2 h. The peak broadening can be seen with increasing milling time which is due to the crystallite size refinement. It is also notable that the NC powder is completely formed at 2 h of milling with a crystallite size less than 30 nm.

3.2. FTIR analysis

FTIR spectra were also recorded for IGT/PVA composite at different percentages of NC. The characteristic band at 3442 cm^{-1} was detected for the stretching frequency of —OH groups as shown in Fig. 4. Asymmetric and symmetric stretching vibrations for methylene groups appeared at around 2930 and 2856 cm^{-1}. A significant band at 1747 cm^{-1} is attributed to —C═O group stretching vibrations. The strong peak at 1495 cm^{-1} is ascribed to characteristic asymmetrical stretch of $—COO^-$ group. The characteristic asymmetrical stretch of $—COO^-$group is caused to appear as bands at 1441 and 1367 cm^{-1}. The spectra showed bands at 11,420 and 1280 cm^{-1}; 1243 and 1100 cm^{-1} for the stretching vibrations of C—O of the polyols, ether and alcohol groups. The strong peak at 1243 cm^{-1} is attributed to stretching vibrations of C—O groups (Fig. 4c). The bands around 2925 and 2854 cm^{-1} 1 are assigned to asymmetric and the symmetric stretching to $—CH_2$ group, respectively. Two peaks at 1737 and 1434 cm^{-1} can be observed for to —CO stretching vibrations: —OH and —CH bending respectively. The absorption peaks at 525 and 450 cm^{-1} are assigned to Si—O—Al and Si—O—Si bonds for tetrahedral bending modes. The intense peak at around 1028 cm^{-1} indicates the Si—O stretching frequencies. Three bending vibrations were considered at 915 cm^{-1} (Al···Al···OH), 747 cm^{-1} (Al···Fe···OH) and 736 cm^{-1} (Al···Mg···OH) due to associated hydroxyl group of bentonite with Al^{+3} cation. In the spectra of PVA/IGT/nanopowder blend nanofibre, the absorption peak at 1617 cm^{-1} is assigned to asymmetrical stretch of $—COO^-$ group which appeared at 1594 cm^{-1} for IGT and shifted to 1618 cm^{-1}

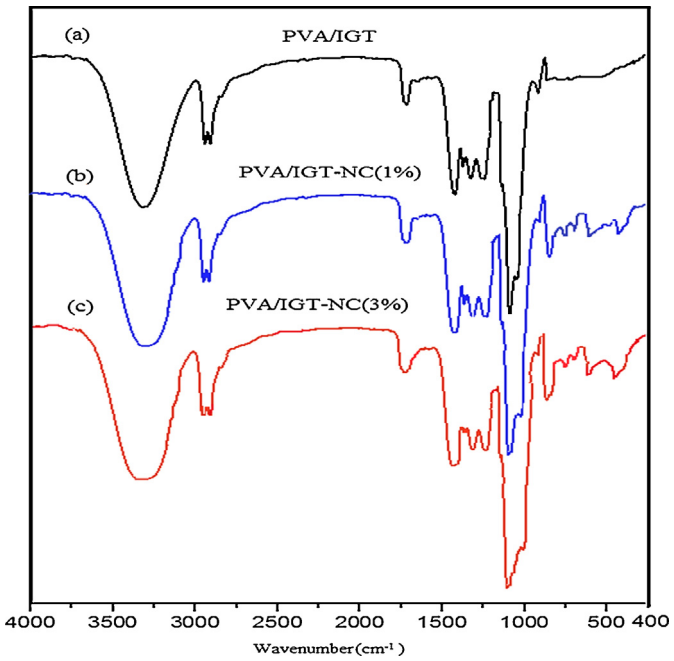

Fig. 4. FTIR spectra of the PVA/IGT with different amount of NC powder (a) 0%, (b) 1%, and (c) 3% in the nanobiocomposite.

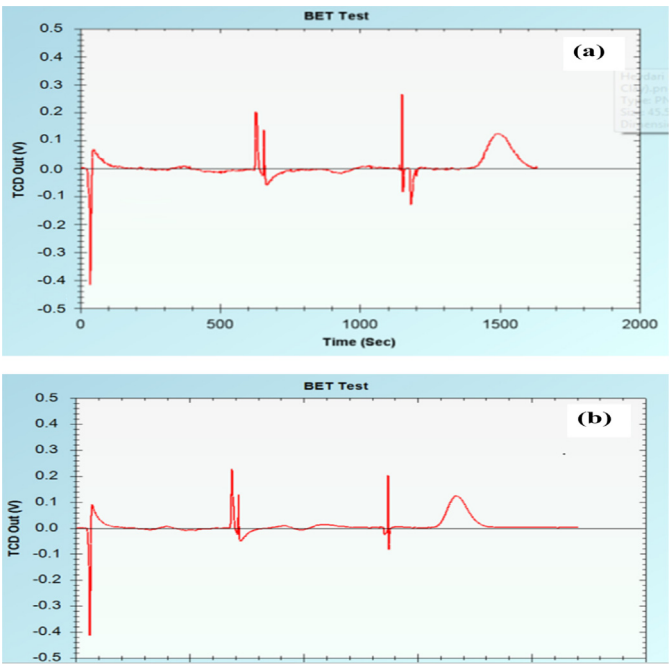

Fig. 5. BET results of the PVA/IGT with different amount of NC powder (a) 1%, and (b) 3% in the nanobiocomposite.

for IGT/PVA nanofibre, suggesting that most of the carboxylic acid groups were associated with intramolecular hydrogen bonding.

3.3. BET analysis

Fig. 5 shows the correlation between the uses of two different ratios of NC in surface porosity. The BET data presented in Table 3 show that the diameter size of nanocomposite decreased from 200 to 50 nm. As is clear from this table, the specific surface area of scaffold increased when the amount of NC reaches 3%. Besides, by increasing the amount of NC powder, the biopolymer diameter decreased from 300 to 120 nm which led to the increase in specific surface area from 5.059 to 6.079 m^2/g. BET results of the PVA/IGT

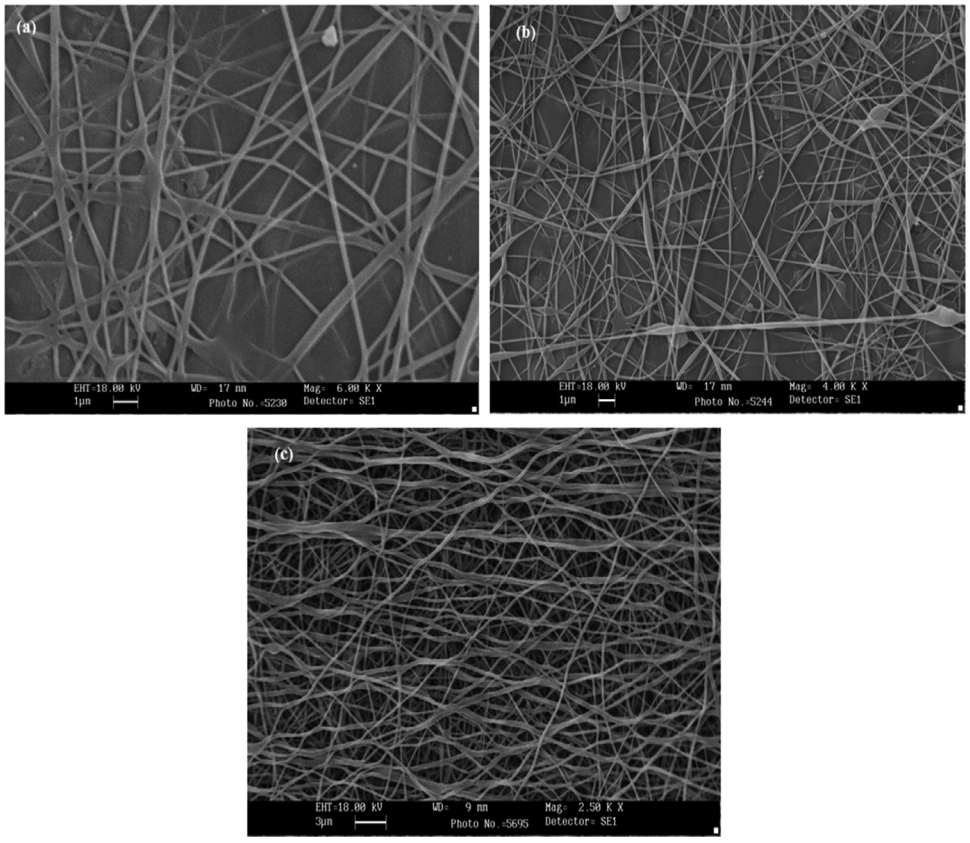

Fig. 6. SEM micrograph of PVA/IGT (20/80) nanofibres (0%, 1%, 3%) before SBF.

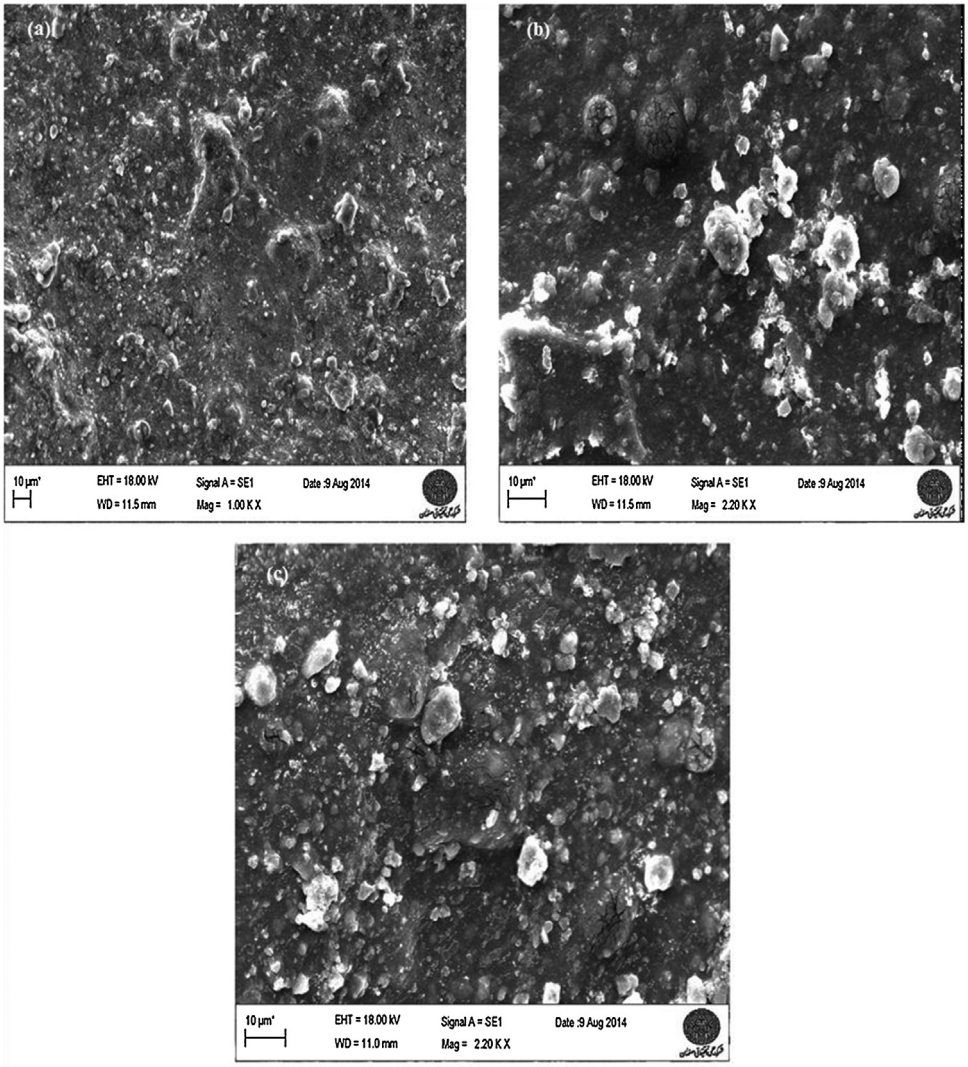

Fig. 7. SEM micrograph of PVA/IGT (20/80) nanofibres; the diameter histogram of corresponding nanofibres analysed (a) 0%, (b) 1%, and (c) 3% after SBF.

with different amount (1% and 3%) of NC powder is shown in Fig. 5a and b in the nanobiocomposite.

3.4. SEM analysis

SEM photomicrographs of the PVA/IGT nanocomposite powders (10/90, 20/80, 30/70, 40/60 samples) at different percentages (0, 1, and 3) of NC are shown in Fig. 6. In the sample fibre of 20/80 with 3% NC, the uniform, randomly oriented nanofibres were obtained. Such fibrous structure would result in a high amount of the surface area to volume ratio and interconnected porosity. A comparison between the SEM images of the sample in the presence and without NC is shown in Fig. 6a–c. It is seen that almost the same surface morphologies were obtained by adding the NC powders, and resulted by the decrease of the inter layer spaces. Images presented in Fig. 7 show that the density of sediments on the surface scaffolds was increased after 28 days of immersion in SBF. The composite containing 3% of NC had the highest bone-like apatite formation which is due to stable state of the NC powder in the SBF solution. SEM images show a relative reduction in particle size and particle size distribution with increasing NC percentage to 3. As can be seen in this figure, there are more hard agglomerates in the composite powders at higher percentage of NC (see Fig. 7). As the percentages of NC powder increases up to 3, the chemical stability of nanofibre also increases.

However, the agglomerates are broken down by increasing the amount of NC (Fig. 7a and c). The event stems from the formation of brittle ceramic phases as a result of increasing NC percentage. According to the SEM analysis, it is obvious that by adding 3% NC nanoparticles, the distribution of nanoparticles in polymer matrix is synchronized. Adding more than 3% NC leads to more gathering of nanoparticles in polymer lattice resulting in the decrease of mechanical properties. SEM micrographs show that the blend nanofibres have a smaller diameter distribution in the presence of more amount of NC.

The nanofibre samples with 3% NC soaked in SBF were characterized by EDX analysis to recognize the presence of the possible elements on their surface (Fig. 8). Recently, silver nanoparticles were directly electrospun into PLLA fibrous membrane by Liu et al. [29]. The result showed that they have a medical potential for reduction of the infection as well as adhesion after tendon injury [29]. EDX analysis of the spot presented on the large white particle shows that it contains mainly carbon, oxygen, sodium, magnesium, phosphorus, chlorine, calcium and silicon. The carbon peak on the EDS spectra stems from the PVA as well as the IGT. The chlorine peaks also come from the HCl solution that was used. Oxygen, sodium, magnesium and calcium are derived from the NC

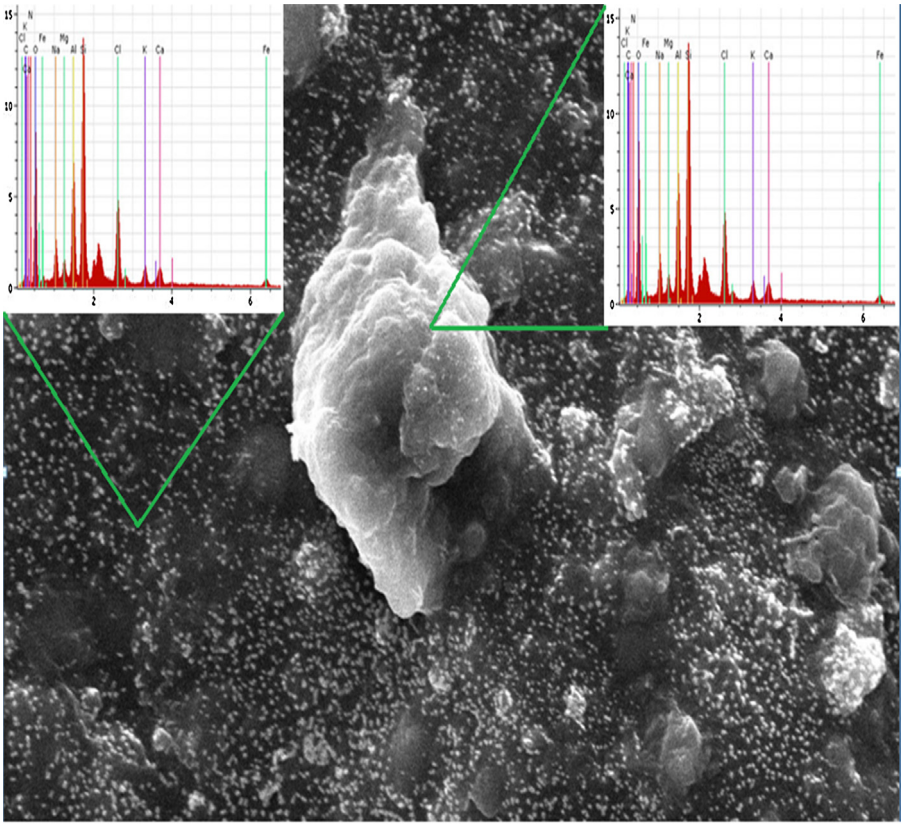

Fig. 8. SEM micrograph and EDS analysis of PVA/IGT (20/80) nanofibres (cauliflower particles); the diameter histogram of corresponding nanofibres analysed 3% of clay after SBF.

particles. Bright spots which appear on the EDX maps illustrate the places with higher concentrations of the studied elements, and also confirm the presence of apatite structure.

The *in vitro* bioactivity is assessed by examination of growth of bone-like apatite on the surface of samples after soaking in Kokubo's SBF solution. Dissolution curves can be very helpful in this area that indicate the changes in calcium ions concentration and pH values *versus* immersion time in SBF (Fig. 9). It is understood from this figure that the pH value as well as Ca ion concentration has decreased during the first two weeks of experiments (Fig. 9). Here, one can say that Ca ions concentration in NC has a higher amount (see XRF analysis for NC in Table 1), leading to instability of the IGT/PVA nanocomposite and hence the entry of calcium ions into the SBF solution. The event leads to the pH decrease in the first two weeks of experiments [25].

As can be observed in Fig. 10, the Ca ions concentration in IGT/PVA is lower than that in IGT/PVA–3% NC nanocomposite

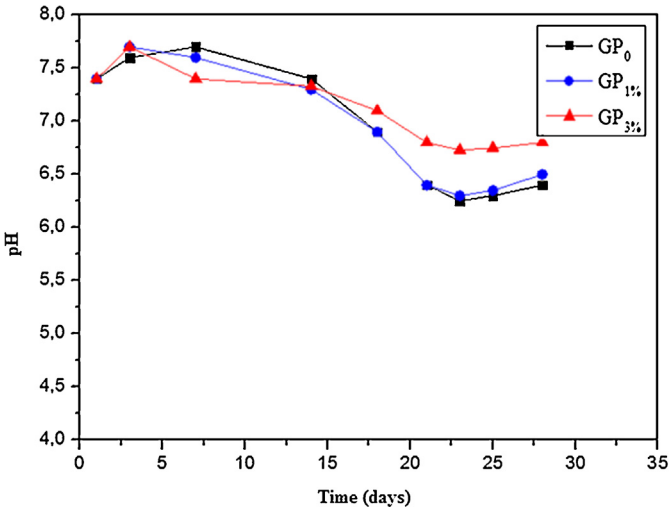

Fig. 9. pH changes of samples immersed in SBF solution in 28 days.

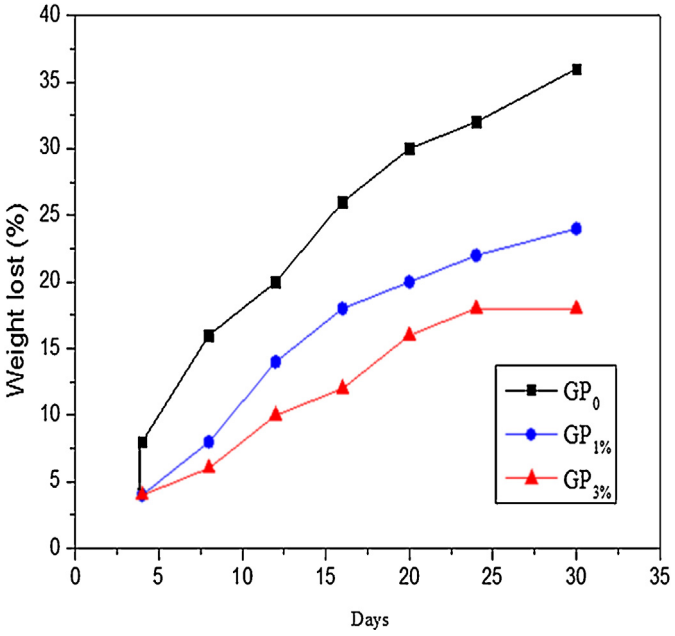

Fig. 10. Weight loss of PVA/IGT (20/80) nanofibres analysed (0%, 1%, 3%) in PBS solution.

samples. This event may be originated from the more density as well as chemical stability of IGT/PVA–3% NC nanocomposite and hence higher reaction with the SBF solution in the first two weeks. In other words, the release of Ca ions from pure IGT/PVA is lower than that from IGT/PVA–3% NC nanocomposite because of its higher chemical stability (see Fig. 10) [25].

3.5. ICP-AES analysis

The concentration of calcium and phosphorous ions existing in the SBF solution after removing the samples from the soaking solution is exhibited in Fig. 10. Due to the increase in amount of nanoclay for GP_3 composition, the concentration values of Ca and P ions decrease from 100 ppm to 92.60 and 40.62 after the 28 days of immersion, respectively. The event originated from the increase of porosity of composite and subsequently strong chemical bond with the bone tissue resulting in the consumption of the phosphorus to form a layer of calcium phosphate on the surface of the fibre composite.

The release of calcium ions from the surface into the SBF solution leads to the formation of many silanol groups on the surface. Silanol groups are heterogeneous nucleation sites for the apatite layers. As can be seen from Fig. 9, the Ca ion concentration begins to decrease for IGT/PVA and tends to be fixed in PVA/IGT–NC nanocomposites after 2 weeks. To explain the event one can say that the SBF solution eventually becomes saturated from the Ca ions (after 2 weeks), so that the calcium ions tend to leave the solution [25]. In other words a balance between the Ca ions release and Ca ions absorption is achieved. It should be noted that there are two places for the absorption of calcium ions [25].

It is clear from Fig. 9 that the optimum amount of pH has been achieved after 28 days for PVA/IGT–NC nanocomposite samples [25].

As the amount of NC increases, the weight loss begins to decrease. Generally, bioceramics improve the chemical stability and mechanical properties of the polymers. As the NC amount increases, the pH value slowly begins to decrease. Fig. 10 shows the curve of PVA/IGT nanofibres containing different amount of NC after degradation for a period of 28 days. This figure shows that by increasing the NC content in the nanocomposite samples, the rate of degradation also increases. The morphology of pure PVA/IGT nanofibre immersed in PBS solution for 28 days showed no changes whereas a considerable degradation was observed for the nanofibres containing 3% NC after 14 days. The increase of degradation rate in the nanocomposite samples is due to this fact that the nanoclay acts as a filler between the polymer chains and so it improves the capability of microorganism growth, and subsequently easier and faster destruction of polymer structure.

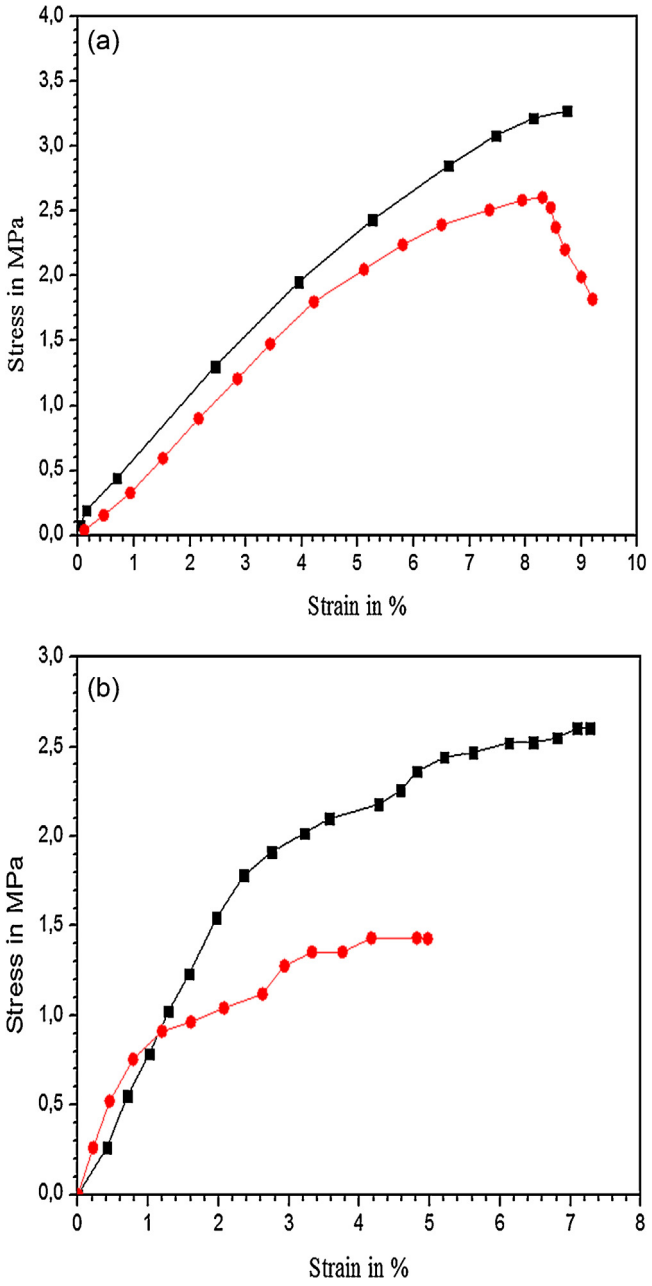

Fig. 11. Stress–strain diagram of PVA/IGT (20/80) nanofibres: (a) the sample without NC and (b) sample with 3% NC.

3.6. Mechanical properties

Mechanical deformation of polymer crystals mostly produces fibres which are observed in electron micrographs of fracture surfaces, for example. Such fibres typically have a diameter less than few tens of nanometres and a length around a few micrometres. The data indicate that when the NC is composited with the IGT/PVA matrix, the produced composite samples achieve a similar level of mechanical stability when applied in the wound healing procedure. As shown in Fig. 11a and b, after entering NC into IGT/PVA solution and electrospinning process, the stronger fibres belong to the samples with higher amount of NC powder. As it can be seen from the graph, the scaffold with 3% NC has a tensile strength that is higher than that without NC, about 40%, which is due to the strengthening nanocomposite samples by ceramic particles. During the study of mechanical properties of PVA/IGT/NC blends, we have found that their nanocomposite samples form clear homogeneous blends in comparison with those in PVA/IGT. This is probably because of the more Young's modulus as well as tensile stress in the later samples [27]. The mechanical property results of PVA/IGT (Fig. 11a) and PVA/IGT/NC (Fig. 11b) blend nanofibres are compared in Fig. 11. As can be seen, the tensile strength and elongation at fracture have increased with increasing NC amount. This approach indicates that there are specific intermolecular interactions between NC and PVA/IGT. Recently, researchers developed different types of soft tissue flexible biodegradable papaverine-loaded electrospun fibrous membranes to be wrapped around vascular suturing for preventing vasospas [28]. Antibacterial agents in the prevention of cell adhesion on repaired tendons of these polymers after injury have also been investigated [29,30] (Table 4).

Table 4
Mechanical analysis of scaffold with and without NC powder, stress, strain, and elastic module.

Result	Max (force) cN	Length change (mm)	Tensile strength (MPa)	Strain (mm)	Elastic module (MPa)
Average GP_0	465.804	1.19	2.03	5.9	87.96
Average GP_3	526.804	1.05	3.83	3.8	9.52

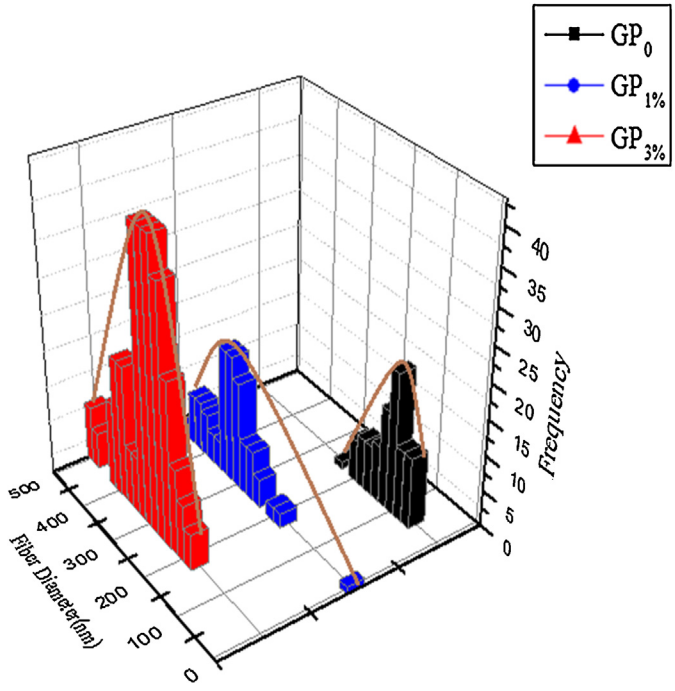

Fig. 12. The diameter histogram of corresponding of PVA/IGT (20/80) nanofibres analysed (0%, 1%, and 3%) after PBS.

3.7. SPSS (statistical)

The results of the statistical analysis ANOVA showed that the average diameter of the fibres which had 0% and 3% of nanoclay were 300 and 120 nm, respectively. The diameter histogram of corresponding nanofibres analysed (10/20/30/40–90/80/70/60 – 1%, 3%) after soaking in the SBF is shown in Fig. 12. As can be seen, as the NC percentage increases, the nanofibres diameter starts to decrease resulting in the increase in the mechanical and chemical stability of the samples.

4. Conclusions

IGT and PVA were blended with the NC powder to improve the spin ability. The IGT/PVA ratio varied during the experiments and the nanofibres with the best morphology were obtained at 20/80 IGT/PVA ratio in the presence of certain amount of NC. According to the results obtained, the average size of nanofibres increased with adding NC powder to the solution. The samples with 3% of NC powder showed excellent bioactivity, biodegradation, and mechanical property compared to the samples with lower amount of NC powder. The obtained results in this research showed that a pure IGT system could not directly be electrospun to yield continuous and uniform nanofibres. To overcome the poor electrospinnability of IGT solution, synthetic polymers such as PVA solution were blended with IGT solution. Furthermore, the blend nanofibres showed advancement in mechanical properties compared to the pure electrospun PVA. The results of FTIR and XRD indicated that there were strong interactions between NC and PVA. Biocompatibility and bioactivity properties of IGT/PVA-3% NC revealed that these nanofibres are suitable for wound healing and can protect the wound surface from the infection as well as dehydration.

References

[1] P. Martin, Science, 276, 75–81 (1997).
[2] G. Chamberlain, J. Fox, B. Ashton and J. Middleton, Stem Cells, 25, 2739–2749 (2007).
[3] T. Mosmann, J. Immunol. Methods, 65, 55–63 (1983).
[4] J.A. Matthews, G.E. Wnek, D.G. Simpson and G.L. Bowlin, Biomacromolecules, 3, 232–238 (2002).
[5] N.A. Peppas and N.K. Mongia, Eur. J. Pharm. Biopharm., 43, 51–58 (1997).
[6] K. Varaprasad, N.N. Reddy, N.M. Kumar, K. Vimala, S. Ravindra and K.M. Raju, Int. J. Polym. Mater., 59, 981–993 (2010).
[7] L. Zhang and A. Eisenberg, Science, 268, 1728–1731 (1995).
[8] A.H. Reddi, J. Cell. Biochem., 56, 192–195 (1994).
[9] N.A. Peppas, J.Z. Hilt, A. Khademhosseini and R. Langer, Adv. Mater., 18, 1345–1360 (2006).
[10] R.L. Depalma, T.M. Krummel, L.A. Durham, B.A. Michna, B.L. Thomas, J.M. Nelson and R.F. Diegelmann, Matrix, 9, 224–231 (1989).
[11] V.G. Kadajji and G.V. Betageri, Polymers, 3, 1972–2009 (2011).
[12] M. Ranjbar-Mohammadi, S.H. Bahrami and M.T. Joghataei, Mater. Sci. Eng. C, 33, 4935–4943 (2013).
[13] M.A. Mohammadifar, S.M. Musavi, A. Kiumarsi and P.A. Williams, Int. J. Biol. Macromol., 38, 31–39 (2006).
[14] F.D. Griffith and J.E. Long, Am. Ind. Hyg. Assoc. J., 41, 576–583 (1980).
[15] V.J. Mkhabela and S.S. Ray, J. Nanosci. Nanotechnol., 14, 535–545 (2014).
[16] C. Zhou, C. Deng, X. Chen, X. Zhao, Y. Chen, Y. Fan and X. Zhang, J. Mech. Behav. Biomed. Mater., 48, 1–11 (2015).
[17] E. Karamian, M.R.K. Motamedi, A. Khandan, P. Soltani and S. Maghsoudi, Prog. Nat. Sci.: Mater. Int., 24, (2) 150–156 (2014).
[18] T. Aboud, Adv. Mater. Res., 1043, 138–144 (2014).
[19] G. Wei, Q. Jin, W.V. and P.X. Ma, Biomaterials, 28, 2087–2096 (2007).
[20] M. Yemini, M. Reches, J. Rishpon and E. Gazit, Nano Lett., 5, 183–186 (2005).
[21] D.H. Reneker, A.L. Yarin, E. Zussman and H. Xu, Adv. Appl. Mech., 41, 43–346 (2007).
[22] X. Zhang, W.J. Goux and S.K. Manohar, J. Am. Chem. Soc., 126, 4502–4503 (2004).
[23] S.V. Dorozhkin, Biomaterials, 31, 1465–1485 (2010).
[24] T. Kokubo and H. Takadama, Biomaterials, 27, 2907–2915 (2006).
[25] H. Gheisari, E. Karamian and M. Abdellahi, Ceram. Int., 41, 5967–5975 (2015).
[26] E. Karamian, A. Khandan, M. Eslami, H. Gheisari and N. Rafiaei, Adv. Mater. Res., 829, 314–318 (2014).
[27] A. Khandan, M. Abdellahi, R.V. Barenji, N. Ozada and E. Karamian, Ceram. Int., 41, 12355–12363 (2015).
[28] W. Zhu, S. Liu, J. Zhao, S. Liu, S. Jiang, B. Li and W. Cui, Acta Biomater., 10, 3018–3028 (2014).
[29] S. Liu, J. Zhao, H. Ruan, W. Wang, T. Wu, W. Cui and C. Fan, Mater. Sci. Eng. C, 33, 1176–1182 (2013).
[30] C. Hu and W. Cui, Adv. Healthcare Mater., 1, 809–814 (2012).